European Journal of Oral Sciences

Eur J Oral Sci 2011; 119 (Suppl. 1): 97–102
DOI: 10.1111/j.1600-0722.2011.00900.x
Printed in Singapore. All rights reserved

European Journal of Oral Sciences

Effect of phosphorylation on the interaction of calcium with leucine-rich amelogenin peptide

Elvire Le Norcy[1,2], Seo-Young Kwak[1,2], Marc Allaire[3], Peter Fratzl[4], Yasuo Yamakoshi[5], James P. Simmer[5], Henry C. Margolis[1,2]

[1]Department of Biomineralization, The Forsyth Institute, Cambridge, MA, USA; [2]Department of Developmental Biology, Harvard School of Dental Medicine, Boston, MA, USA; [3]National Synchrotron Light Source, Brookhaven National Laboratory, Upton, NY, USA; [4]Department of Biomaterials, Max Planck Institute of Colloids and Interfaces, Research Campus Golm, Potsdam, Germany; [5]Department of Biologic and Materials Sciences, University of Michigan School of Dentistry, Ann Arbor, MI, USA

Le Norcy E, Kwak S-Y, Allaire M, Fratzl P, Yamakoshi Y, Simmer JP, Margolis HC. Effect of phosphorylation on the interaction of calcium with leucine-rich amelogenin peptide.
Eur J Oral Sci 2011; 119 (Suppl. 1): 97–102. © 2011 Eur J Oral Sci

Amelogenin undergoes self-assembly and plays an essential role in guiding enamel mineral formation. The leucine-rich amelogenin peptide (LRAP) is an alternative splice product of the amelogenin gene and is composed of the N terminus (containing the only phosphate group) and the C terminus of full-length amelogenin. This study was conducted to investigate further the role of phosphorylation in LRAP self-assembly in the presence and absence of calcium using small angle X-ray scattering (SAXS). Consistent with our previous dynamic light-scattering findings for phosphorylated (+P) and non-phosphorylated (−P) LRAP, SAXS analyses revealed radii of gyration (R_g) for LRAP(−P) (46.3–48.0 Å) that were larger than those for LRAP(+P) (25.0–27.4 Å) at pH 7.4. However, added calcium (up to 2.5 mM) induced significant increases in the R_g of LRAP(+P) (up to 46.4 Å), while it had relatively little effect on LRAP(−P) particle size. Furthermore, SAXS analyses suggested compact folded structures for LRAP(−P) in the presence and absence of calcium, whereas the conformation of LRAP(+P) changed from an unfolded structure to a more compact structure upon the addition of calcium. We conclude that the single phosphate group in LRAP(+P) induces functionally important conformational changes, suggesting that phosphorylation may also influence amelogenin conformation and protein–mineral interactions during the early stages of amelogenesis.

Henry C. Margolis, Department of Biomineralization, The Forsyth Institute, 245 First Street, Cambridge, MA 02142, USA

Telefax: +1–617–8928432
E-mail hmargolis@forsyth.org

Key words: amelogenin; conformation; leucine-rich amelogenin peptide; phosphorylation; small angle X-ray scattering

Accepted for publication September 2011

Enamel is the most highly mineralized vertebrate tissue, composed of ~96% mineral and 4% organic material and water. During amelogenesis, the ameloblast secretes matrix proteins and is responsible for creating and maintaining an extracellular environment favorable for mineral deposition (1). Amelogenin, the predominant enamel matrix protein, has been shown to undergo self-assembly to form spherical or oblate-shaped nanoparticles (2–4), as well as elongated structures (5–7), and is believed to play an essential role in guiding the formation of ordered arrays of apatitic crystals during enamel development (5, 8–12). In particular, both the N-terminal domain (containing the only phosphate group on serine 16) and the hydrophilic C-terminal domain of full-length amelogenin (Fig. 1) have been shown to be critical for proper enamel formation (13–16). It is also believed that during enamel mineral growth, the concentration of free calcium ions is regulated, in part, by the binding of calcium to enamel proteins and their proteolytic cleavage products (17, 18).

The leucine-rich amelogenin peptide (LRAP), a 56-amino-acid alternative splice product of the amelogenin gene found throughout amelogenesis and composed of the first 33 N-terminal and the last 23 C-terminal amino acids of full-length amelogenin (Fig. 1), has recently been shown by us to share similar behavioral properties with amelogenin with respect to self-assembly and its ability to regulate crystal growth *in vitro* (19, 20). As in solution (19), LRAP has also been shown to assemble into nanospheres on fluoroapatite (21) and on surfactant-coated gold surfaces (22). Furthermore, it has been shown (23) that non-phosphorylated LRAP [LRAP(−P)] and recombinant full-length human amelogenin (rH174) have the same capacity to bind calcium (i.e. four to six calcium ions per molecule), although the calcium affinity constant for LRAP was greater than that for the full-length amelogenin. Based on similarities of structure and behavior, LRAP has allowed us to investigate the potential role of specific amino-acid domains of amelogenin and phosphorylation in protein self-assembly using dynamic light scattering (DLS) and transmission electron microscopy (TEM). Such studies have illustrated potentially important differences in the self-assembly behavior of phosphorylated LRAP [(LRAP(+P)] and LRAP(−P) (19).

The aim of the present study was to extend these recent findings using small angle X-ray scattering (SAXS), to investigate further the role of phosphorylation in LRAP self-assembly, in the presence and absence of calcium, through comparative studies of LRAP(+P) and LRAP(−P) forms of LRAP (Fig. 1).

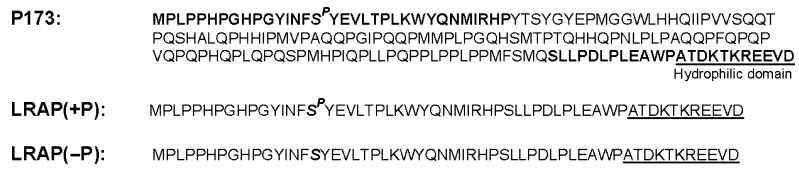

Fig. 1. Amino-acid sequences of the full-length porcine amelogenin (P173) and the phosphorylated (+P) and non-phosphorylated (−P) leucine-rich amelogenin peptide (LRAP). Note that LRAP is composed exclusively of the N- and C-terminal domains (shown in bold type) of the full-length molecule.

Material and methods

Preparation of amelogenin peptides

LRAP(+P) and LRAP(−P) forms of porcine LRAP (56 amino acids) were synthesized commercially (NEO Peptide, Cambridge, MA, USA) and purified as previously described (24). Lyophilized peptides were weighed and dissolved in distilled deionized water at room temperature to yield stock solutions of 5–6 mg ml^{-1} of peptide. The solutions were kept at room temperature for 30 min and then stored at 4°C for 24 h before checking complete dissolution by DLS. Peptide stock solutions were centrifuged (10,900 × *g*, 4°C, 20 min) just before use.

SAXS measurements

Aliquots of peptides were adjusted to a pH of ~7.4 with small amounts of KOH and HCl to obtain final concentrations of 2 mg ml^{-1} (0.31 mM) and 5 mg ml^{-1} (0.76 mM) of LRAP (total volume 70 μl). In selected experiments, calcium chloride was added to peptide solutions before adjustment of pH to yield final concentrations of 0.76–2.5 mM calcium (total volume = 70 μl). Hence, on a molar basis, the calcium to protein ratios ranged from 1.0 to 8.1. All sample preparations were carried out at room temperature.

Solution X-ray scattering experiments were carried out at the National Synchrotron Light Source at Brookhaven National Laboratory, on beamline X9 (25). The X-ray wavelength was 0.918 Å and the sample-detector distance was 3.4 m. The sample holder was a 0.9-mm-diameter quartz capillary tube that was open at both ends to allow continuous flow of the sample to avoid X-ray damage. Each measurement required 15 μl of sample and an exposure time of 30 s at 13°C. Triplicate measurements were conducted for each experiment. The two-dimensional images acquired on a PILATUS 300K detector (Dectris, Baden, Switzerland) were averaged into one-dimensional scattering curves and then water scattering was subtracted using the pyXS software developed at the beamline. Solution X-ray scattering data were further analyzed using Primus software (26). The data consisted of the scattering vector, s [defined as $s = 2\pi/d$ or $4\pi\sin(\theta)/\lambda$], and the corresponding intensity, $I(s)$. As noted in the Results section, Guinier and Kratky plots were used to analyze the data. Guinier analyses consisted of the plotting of log I vs. s^2 at very low s values and were used to determine the radius of gyration, R_g, and the extrapolated intensity at the zero scattering angle, I_o, with R_g being the mass distribution of the macromolecule around its center of gravity (27). Kratky analyses were carried out by plotting $I(s) \times s^2$ vs. s and provided information on peptide folding, as described later (28). The number of molecules per particle was estimated using the following formula: $N = (V_S \times N_A \times \delta_p)/F_W$; where, $V_S = (4\pi R_g^3)/3$, the density of the protein $\delta_p = 1.44$ g cm^{-3} (3), N_A is the Avogadro constant, and $F_W = 6537.52$ Da.

Results

Size of particles formed

Small angle X-ray scattering enables determination of the molecular size, shape, and conformational change of a protein molecule in solution. As shown in Fig. 2, the scattering generally exhibited fairly good linear dependence [log $I(s)$ vs. s^2] at low s, indicating little to no bulk aggregation and allowing further data processing. As shown in Table 1, Guinier plots revealed that the R_g was 48.0 ± 0.05 Å for LRAP(−P) but only 25.0 ± 0.50 Å for LRAP(+P) (both at 2 mg ml^{-1}, 13°C, pH 7.4), in the absence of added calcium. The R_g values for each peptide were very similar when the peptide concentration was increased to 5 mg ml^{-1}, with an R_g of 46.3 ± 0.02 Å for LRAP(−P) and an R_g of 27.4 ± 0.08 Å for LRAP(+P), under the same experimental conditions. The addition of 2.5 mM calcium to 2 mg ml^{-1} solutions of peptide, however, induced a significant increase in the R_g for LRAP(+P) to 43.9 ± 0.05 Å, but it had relatively little effect on the R_g of LRAP(−P), with a value of 46.2 ± 0.03 Å being determined (Table 1). Similar results were obtained for 5 mg ml^{-1} peptide solutions containing 2.5 mM calcium, yielding R_g values for LRAP(+P) and LRAP(−P) of 46.4 ± 0.06 Å and 53.9 ± 0.06 Å, respectively. As also shown in Table 1, using peptide concentrations of 5 mg ml^{-1}, increasing concentrations of calcium added to LRAP(−P) solutions resulted in a progressive, but slight, increase in the R_g values, whereas increased calcium concentrations resulted in marked concentration-dependent increases in the R_g values for LRAP(+P).

Increased I_o values per unit peptide concentration (c), I_o/c (Table 1), calculated for the LRAP(+P) samples, however, were consistent with peptide self-assembly (29), as particle sizes (R_g) increased by an overall factor of around two upon the addition of higher concentrations of calcium. In contrast, as clearly seen in 5 mg ml^{-1} samples, a much smaller increase in I_o/c was observed for LRAP(−P) upon the addition of calcium. Similar increases in the number of molecules per particle were also observed (Table 1). Overall, under comparable conditions, I_o values were larger for LRAP(−P) than for LRAP(+P) and corresponded to a somewhat greater number of molecules per particle.

Determination of conformational changes

Kratky plots [$I(s) \times s^2$ vs. s] of SAXS data present characteristic and distinctly different shapes for globular fol-

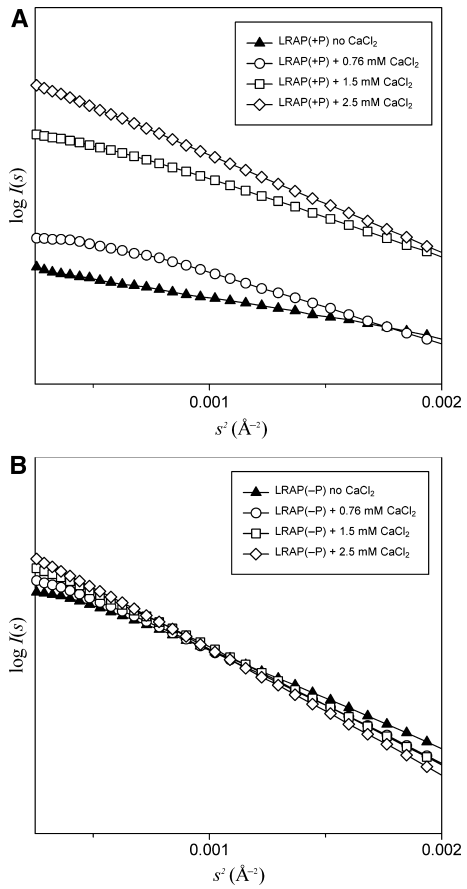

Fig. 2. The Guinier region of the scattering curve for phosphorylated leucine-rich amelogenin peptide [LRAP(+P)] (A) and non-phosphorylated leucine-rich amelogenin peptide [LRAP(−P)] (B) data recorded in the absence and in the presence of 0.76–2.5 mM calcium chloride ($CaCl_2$). Curves in (A) and (B) exhibit fairly good linear dependence of log $I(s)$ vs. s^2, indicating little to no bulk aggregation. Data shown are for 5 mg ml^{-1} peptide concentrations. $I(s)$, intensity of s; s, scattering vector.

ded molecules and extended-chain or random-coil molecules of similar molecular mass (30–32). Globular macromolecules follow Porod's law and have bell-shaped curves as the clearly defined surface of the protein leads to a drop in intensity with the fourth power of s (31), whereas extended molecules, such as unfolded peptides, lack this peak and have a plateau or increase slightly in the larger s range. As shown in Fig. 3A,B,D, the Kratky plot of LRAP(−P) data in the absence of calcium showed a bell-shaped curve, indicating a globular structure. The addition of up to 2.5 mM calcium did not induce an apparent conformational change, as LRAP(−P) exhibited similar bell-shaped curves in the presence of various concentrations of calcium (0.76–2.5 mM), as it did in its absence (Fig. 3A,B,D). On the contrary, in the absence of calcium, LRAP(+P) showed a plateau indicating an unfolded extended random structure (Fig. 3A–C). However, a prominent peak appeared upon the addition of 2.5 mM calcium, suggesting the formation of a more globular LRAP(+P)–Ca structure (Fig. 3A,B). The extent of folding of the LRAP(+P) peptide was also found to be dependent upon the concentration of calcium added (Fig. 3C). The addition of 0.76 mM calcium induced the formation of a very slight peak, suggesting that the peptide remained mostly in the unfolded state with the appearance of some globular features; upon the addition of 1.5 mM calcium the peak appeared more pronounced, indicating an increase in peptide folding. With the addition of 2.5 mM calcium, the peak of the Kratky plot for LRAP(+P) became even more pronounced and began to resemble that of the non-phosphorylated LRAP(−P) peptide, although the curves remained somewhat distinct at higher values of s (Fig. 3A–D).

Discussion

Leucine-rich amelogenin peptide, like amelogenin, is a phosphorylated protein that is secreted with a single phosphate group on serine 16 (33). Previous studies from our laboratory have shown that this single phosphate group has a major influence on the properties of amelogenin. In particular, in comparison with their non-phosphorylated (recombinant or synthetic) counterparts, phosphorylated (native and synthetic) forms of full-length porcine amelogenin (P173) (7), truncated porcine amelogenin P148 (8), full-length LRAP(+P) (19), and a truncated form of LRAP [LRAP(+P,−CT] (20) all exhibit the capacity to stabilize amorphous calcium phosphate (ACP) effectively [i.e. prevent its transformation to crystalline hydroxyapatite (HA)], under experimental conditions designed to support the spontaneous formation of calcium phosphates *in vitro*. In sharp contrast to these findings, non-phosphorylated forms of full-length amelogenin and full-length LRAP were shown to guide the formation of ordered bundles of apatitic crystals (5, 8, 19). This latter behavior has been attributed to the ability of full-length amelogenin (6, 7, 15, 34) and LRAP (19) to form higher-order chain-like structures under specified conditions of pH. The presence of calcium has also previously been shown to enhance the formation of chain-like structures of recombinant full-length mouse rM179 (5) and human rH174 (35), amelogenin, and LRAP (19). Notably, as shown in the latter study, particle sizes and the formation of chain-like structures were enhanced to a greater degree for the phosphorylated form of LRAP. This conclusion was based on DLS and TEM observations. Our present SAXS findings support this conclusion and further demonstrate that the presence of calcium has a profound effect on the size and conformation of LRAP(+P) and little effect on those characteristics of LRAP(−P). This effect is caused by the presence of a single phosphate group on serine 16.

Guinier (Table 1) and Kratky (Fig. 3) analyses revealed further assembly and enhanced folding of LRAP(+P) upon the addition of calcium (Fig. 3A–C). Further assembly with added calcium is indicated (Table 1) by marked increases in R_g values, in estimates of the number of molecules per particle, and in I_o/c values. However, it should be noted that I_o values are affected by factors other than particle size (i.e. R_g), such as particle shape and particle density, in the proportion

Table 1
Guinier analyses of effect of peptide and calcium concentrations on particle size

Peptide concentration	[$CaCl_2$] (mM)	Guinier				Number of molecules per particle
		R_g (Å)	Error	I_o	I_o/c	
2 mg ml^{-1}						
LRAP(+P)	0	25.0	0.489	8.39	4.2	9
	2.5	43.9	5.34E-02	73.12	36.6	47
LRAP(−P)	0	48.0	5.34E-02	100.33	50.2	61
	2.5	46.2	2.59E-02	85.87	42.9	55
5 mg ml^{-1}						
LRAP(+P)	0	27.4	7.77E-02	20.304	4.06	11
	0.76	35.5	5.32E-02	51.829	10.4	25
	1.5	40.7	4.08E-02	115.14	23.0	37
	2.5	46.4	6.41E-02	165.03	33.0	56
LRAP(−P)	0	46.3	2.20E-02	230.17	46.0	55
	0.76	49.5	2.80E-02	254.58	50.9	67
	1.5	52.0	4.30E-02	286.57	57.3	78
	2.5	53.9	6.24E-02	302.99	60.6	87

LRAP(−P) and LRAP(+P) exhibit similar radii of gyration (R_g) at 2 and 5 mg ml^{-1}. The R_g of LRAP(+P) is half that of LRAP(−P) in the absence of calcium at pH∼7.4. R_g and I_o/c for LRAP(−P) increased slightly upon the addition of up to 2.5 mM calcium, whereas marked and progressive increases in these parameters were observed in the presence of LRAP(+P), upon the addition of calcium. The estimated number of molecules calculated from the R_g is presented for comparison purposes.
I_o, the extrapolated intensity at zero scattering angle; I_o/c, the I_o value per unit peptide concentration; LRAP, leucine-rich amelogenin peptide; LRAP(−P), non-phosphorylated leucine-rich amelogenin peptide; LRAP(+P), phosphorylated leucine-rich amelogenin peptide.

$I_o/c \propto (\rho_{particle}-\rho_{solvent})^2 \times V_{particle}$, where ρ indicates (electron) density and $V_{particle}$ indicates the volume of a single particle (27). Although our present analyses do not take potential differences in these latter factors into consideration, LRAP(+P) and LRAP(−P) were found to behave quite differently in the absence and presence of calcium, particularly with respect to folding. In contrast to that seen with LRAP(+P), as observed previously using circular dichroism (36), LRAP(−P) does not undergo significant conformational change upon the addition of calcium (Fig. 3A,B,D). Moreover, as demonstrated here (Fig. 3), LRAP(+P) exhibits a more unfolded structure than LRAP(−P), particularly in the absence and presence of lower concentrations of calcium. It appears that in the presence of calcium, unfolded LRAP(+P) molecules assemble to form more globular-like structures and the process is primarily triggered by calcium concentration (Table 1 and Fig. 3). As seen in Fig. 3, however, differences in Kratky plots for LRAP(+P) and LRAP(−P), which persist even in the presence of the highest calcium concentration studied at high *s* values, suggest that LRAP(+P) remains somewhat more unfolded than LRAP(−P) under these conditions. Additional studies will be needed to provide insight into other potential differences in LRAP(+P) and LRAP(−P) self-assembly, as briefly noted above.

The remarkable conformational difference between LRAP(+P) and LRAP(−P) shown here offers a possible explanation for the differences observed in assembly behavior and for the effects that these peptides have on calcium phosphate precipitation *in vitro*. Changes in the folding of LRAP(+P), induced by the addition of calcium, may result from favorable calcium interactions with specific peptide sites that are exposed in the less-folded LRAP(+P) molecules. Such interactions lead to an enhancement of protein–protein interactions and to the formation of higher-order anisotropic chain-like structures (19). Hence, based on our present findings, it is concluded that the presence of the single phosphate group in LRAP induces functionally important conformational changes in the protein structure that favor the formation of higher-order protein assemblies. Accordingly, specific structure-changing calcium interactions that take place with LRAP(+P) do not occur with the non-phosphorylated LRAP(−P), as LRAP(−P) is inherently more tightly folded and key calcium-binding sites are concealed. Furthermore, observed differences in folding, and the tendency for LRAP(+P) to form less folded structures in the absence and presence of calcium, may also explain why phosphorylated LRAP(+P) is much more effective in stabilizing ACP nanoparticles and preventing the transformation of ACP into HA. The more open structure and the calcium-induced folding of LRAP(+P), in the presence of calcium and phosphate under mineralizing conditions, could lead to a more effective sequestration of forming ACP nanoparticles that prevents the transformation of ACP to HA. The fact that LRAP(−P) has been shown to stabilize ACP only transiently (19) is consistent with the present findings and this developing hypothesis on the effect of phosphorylation on protein conformation and mineralization. However, it is important to consider that previous findings also show that LRAP(−P) (19), like the full-length non-phosphorylated amelogenins rM179 (5) and rP172 (8), has the capacity to regulate the formation of ordered arrays of apatitic crystals by guiding the alignment, fusion, and subsequent transformation of the initially formed ACP nanoparticles (8). This capability

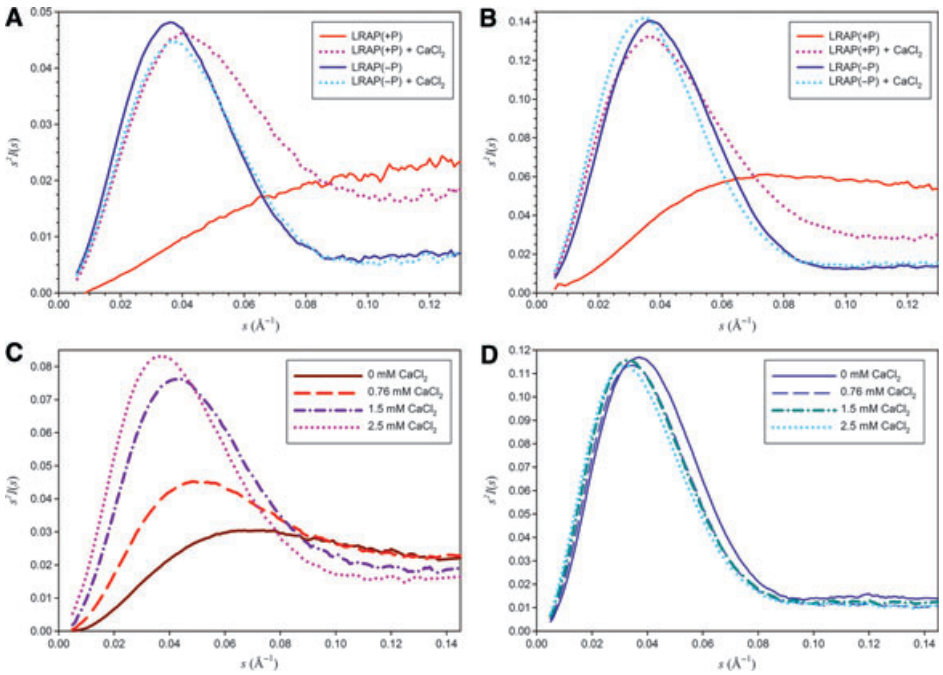

Fig. 3. Small angle X-ray scattering (SAXS) analyses of non-phosphorylated leucine-rich amelogenin peptide [LRAP(−P)] and phosphorylated leucine-rich amelogenin peptide [LRAP(+P)]. Kratky plots of LRAP(−P) and LRAP(+P) at 2 mg ml^{-1} (A) and 5 mg ml^{-1} (B–D) were determined in the absence and in the presence of 2.5 mM $CaCl_2$ (A and B) and from 0 to 2.5 mM $CaCl_2$ (C and D). The plots of LRAP(−P) in the absence and presence of calcium showed a similar bell-shaped curve, indicating globular structures (A, B and D). However, in the absence of calcium (A and B), LRAP(+P) showed a plateau indicating an unfolded structure, whereas a prominent peak appeared upon the addition of 2.5 mM calcium (A and B). This latter peak was found to become increasingly more pronounced as a function of calcium concentration (C), suggesting the formation of a more globular LRAP(+P) structure in the presence of added calcium. $I(s)$, intensity of s; s, scattering vector.

was found to depend on the presence of the hydrophilic C terminus in both amelogenin and LRAP (20). Based on these collective findings, additional processes [e.g. proteolysis or dephosphorylation, as we have recently discussed (19)] may be involved *in vivo* to trigger the subsequent transformation of initially formed ACP particles, as found in the early stages of developing enamel (37). We propose that initially formed ACP mineral in developing enamel is stabilized by native phosphorylated amelogenins that guide the accumulation and linear arrangement of amorphous nanoparticles which serve as precursors to enamel crytallites.

In conclusion, we have shown that the single phosphate group in LRAP(+P) induces functionally important conformational changes, particularly with respect to calcium interactions. Although further studies are needed, the present findings suggest that phosphorylation may also influence amelogenin conformation and subsequent protein–mineral interactions during the early stages of amelogenesis.

Acknowledgement – This work was supported by grant DE-016376 (to H.C.M) from the National Institute of Dental and Craniofacial Research. Use of beamline X9 and the National Synchrotron Light Source, Brookhaven National Laboratory, was supported by the US Department of Energy, Office of Science, Office of Basic Energy Sciences, under contract no. DE-AC02-98CH10886.

Conflicts of interest – The authors declare that there are no conflicts of interest with respect to this manuscript.

References

1. Nanci A. Enamel: composition, formation and structure. In: Nanci, ed. *Ten Cate*'s oral histology – development, structure, and function, 7th edn. St Louis: Mosby Inc., 2008; 141–190.
2. Aichmayer B, Margolis HC, Sigel R, Yamakoshi Y, Simmer JP, Fratzl P. The onset of amelogenin nanosphere aggregation studied by small-angle X-ray scattering and dynamic light scattering. *J Struct Biol* 2005; **151**: 239–249.
3. Aichmayer B, Wiedemann-Bidlack FB, Gilow C, Simmer JP, Yamakoshi Y, Emmerling F, Margolis HC, Fratzl P. Amelogenin nanoparticles in suspension: deviations from spherical shape and pH-dependent aggregation. *Biomacromolecules* 2010; **11**: 369–376.
4. Fincham AG, Moradian-Oldak J, Diekwisch TGH, Lyaruu DM, Wright JT, Bringas JRP, Slavkin HC. Evidence for amelogenin "nanospheres" as functional components of secretory-stage enamel matrix. *J Struct Biol* 1995; **115**: 50–59.
5. Beniash E, Simmer JP, Margolis HC. The effect of recombinant mouse amelogenins on the formation and organization of hydroxyapatite crystals in vitro. *J Struct Biol* 2005; **149**: 182–190.
6. Wiedemann-Bidlack FB, Beniash E, Yamakoshi Y, Simmer JP, Margolis HC. pH triggered self-assembly of native and recombinant amelogenins under physiological pH and temperature in vitro. *J Struct Biol* 2007; **160**: 57–69.
7. Wiedemann-Bidlack FB, Kwak SY, Beniash E, Yamakoshi Y, Simmer JP, Margolis HC. Effects of phosphorylation on the self-assembly of native full-length porcine amelogenin and its regulation of calcium phosphate formation in vitro. *J Struct Biol* 2011; **173**: 250–260.
8. Kwak SY, Wiedemann-Bidlack FB, Beniash E, Yamakoshi Y, Simmer JP, Litman A, Margolis HC. Role of 20-kDa amelogenin (P148) phosphorylation in calcium phosphate formation in vitro. *J Biol Chem* 2009; **284**: 18972–18979.

9. Margolis HC, Beniash E, Fowler CE. Role of macromolecular assembly of enamel matrix proteins in enamel formation. *J Dent Res* 2006; **85**: 775–793.
10. Moradian-Oldak J, Tan J, Fincham AG. Interaction of amelogenin with hydroxyapatite crystals: an adherence effect through amelogenin molecular self-association. *Biopolymers* 1998; **46**: 225–238.
11. Tarasevich BJ, Howard CJ, Larson JL, Snead ML, Simmer JP, Paine M, Shaw WJ. The nucleation and growth of calcium phosphate by amelogenin. *J Cryst Growth* 2007; **304**: 407–415.
12. Wang L, Guan X, Du C, Moradian-Oldak J, Nancollas GH. Amelogenin promotes the formation of elongated apatite microstructures in a controlled crystallization system. *J Phys Chem C nanomater interfaces* 2007; **111**: 6398–6404.
13. Paine ML, Snead ML. Protein interactions during assembly of the enamel organic extracellular matrix. *J Bone Miner Res* 1997; **12**: 221–227.
14. Paine ML, Luo W, Zhu DH, Bringas JRP, Snead ML. Functional domains for amelogenin revealed by compound genetic defects. *J Bone Miner Res* 2003; **18**: 466–472.
15. Paine ML, Wang HJ, Snead ML. Amelogenin self-assembly and the role of the proline located within the carboxyl-teleopeptide. *Connect Tissue Res* 2003; **44** (Suppl 1): 52–57.
16. Pugach MK, Li Y, Suggs C, Wright JT, Aragon MA, Yuan ZA, Simmons D, Kulkarni AB, Gibson CW. The amelogenin C-terminus is required for enamel development. *J Dent Res* 2010; **89**: 165–169.
17. Yamakoshi Y, Tanabe T, Oida S, Hu CC, Simmer JP, Fukae M. Calcium binding of enamel proteins and their derivatives with emphasis on the calcium-binding domain of porcine sheathlin. *Arch Oral Biol* 2001; **46**: 1005–1014.
18. Aoba T, Moreno EC. The enamel fluid in the early secretory stage of porcine amelogenesis: chemical composition and saturation with respect to enamel mineral. *Calcif Tissue Int* 1987; **41**: 86–94.
19. Le Norcy E, Kwak SY, Wiedemann-Bidlack FB, Beniash E, Yamakoshi Y, Simmer JP, Margolis HC. Leucine-rich amelogenin peptides regulate mineralization in vitro. *J Dent Res* 2011; **90**: 1091–1097.
20. Le Norcy E, Kwak SY, Wiedemann-Bidlack FB, Beniash E, Yamakoshi Y, Simmer JP, Margolis HC. Potential role of the amelogenin N-terminus in the regulation of calcium phosphate formation in vitro. *Cells Tissues Organs* 2011; **194**: 188–193.
21. Habelitz S, Denbesten PK, Marshall SJ, Marshall GW, Li W. Self-assembly and effect on crystal growth of the leucine-rich amelogenin peptide. *Eur J Oral Sci* 2006; **114** (Suppl 1): 315–319.
22. Tarasevich BJ, Lea S, Shaw WJ. The leucine rich amelogenin protein (LRAP) adsorbs as monomers or dimers onto surfaces. *J Struct Biol* 2010; **169**: 266–276.
23. Le TQ, Gochin M, Featherstone JD, Li W, Denbesten PK. Comparative calcium binding of leucine-rich amelogenin peptide and full-length amelogenin. *Eur J Oral Sci* 2006; **114** (Suppl 1): 320–326.
24. Nagano T, Kakegawa A, Yamakoshi Y, Tsuchiya S, Hu JC, Gomi K, Arai T, Bartlett JD, Simmer JP. Mmp-20 and Klk4 cleavage site preferences for amelogenin sequences. *J Dent Res* 2009; **88**: 823–828.
25. Allaire M, Yang L. Biomolecular solution X-ray scattering at the National Synchrotron Light Source. *J Synchrotron Radiat* 2011; **18**: 41–44.
26. Konarev PV, Volkov VV, Sokolova AV, Koch MHJ, Svergun DI. PRIMUS: a Windows PC-based system for small-angle scattering data analysis. *J Appl Cryst* 2003; **36**: 1277–1282.
27. Guinier A, Fournet G. *Small-angle scattering of X-rays*. New York: Wiley, 1955.
28. Glatter O, Kratky O, eds. *Small-angle X-ray scattering*. London: Academic Press, 1982.
29. Kearney KR, Moore PB. X-ray solution-scattering studies of active and inactive *Escherichia coli* ribosomal subunits. *J Mol Biol* 1983; **170**: 381–402.
30. Semisotnov GV, Kihara H, Kotova NV, Kimura K, Amemiya Y, Wakabayashi K, Serdyuk IN, Timchenko AA, Chiba K, Nikaido K, Ikura T, Kuwajima K. Protein globularization during folding. A study by synchrotron small-angle X-ray scattering. *J Mol Biol* 1996; **262**: 559–574.
31. Doniach S. Changes in biomolecular conformation seen by small angle X-ray scattering. *Chem Rev* 2001; **101**: 1763–1778.
32. Putnam CD, Hammel M, Hura GL, Tainer JA. X-ray solution scattering (SAXS) combined with crystallography and computation: defining accurate macromolecular structures, conformations and assemblies in solution. *Q Rev Biophys* 2007; **40**: 191–285.
33. Fincham AG, Moradian-Oldak J, Sarte PE. Mass-spectrographic analysis of a porcine amelogenin identifies a single phosphorylated locus. *Calcif Tissue Int* 1994; **55**: 398–400.
34. Buchko GW, Tarasevich BJ, Bekhazi J, Snead ML, Shaw WJ. A solution NMR investigation into the early events of amelogenin nanosphere self-assembly initiated with sodium chloride or calcium chloride. *Biochemistry* 2008; **47**: 13215–13222.
35. He X, Wu S, Martinez-Avila O, Cheng Y, Habelitz S. Self-aligning amelogenin nanoribbons in oil-water system. *J Struct Biol* 2011; **174**: 203–212.
36. Shaw WJ, Ferris K. Structure, orientation, and dynamics of the C-terminal hexapeptide of LRAP determined using solid-state NMR. *J Phys Chem B* 2008; **112**: 16975–16981.
37. Beniash E, Metzler RA, Lam RSK, Gilbert PUPA. Transient amorphous calcium phosphate in forming enamel. *J Struct Biol* 2009; **166**: 133–143.